Integrative Biology

PAPER

View Article Online
View Journal

Cite this: DOI: 10.1039/c5ib00092k

Modeling the finger instability in an expanding cell monolayer†

Victoria Tarle,[a] Andrea Ravasio,[b] Vincent Hakim[c] and Nir S. Gov[a]

Received 15th April 2015,
Accepted 7th June 2015

DOI: 10.1039/c5ib00092k

www.rsc.org/ibiology

Collective motion occurs in many biological processes, such as wound healing, tumor invasion and embryogenesis. Experiments of cell monolayer migration have revealed the spontaneous formation of finger-like instabilities, with leader cells at their tips. We present a particle-based model for collective cell migration, based on several elements that have been found experimentally to influence cellular movement. Inside the bulk we include velocity alignment interactions between neighboring cells. At the border contour of the layer we introduce the following additional forces: surface-elasticity restoring force, curvature-dependent positive feedback, and contractile acto-myosin cables. We find that the curvature-driven instability at the layer edge is necessary and sufficient for the formation of cellular fingers, which are in good agreement with experimental observations.

Insight, innovation, integration

Collective cell motion occurs in many biological processes, such as wound healing, tumor invasion and embryogenesis. Experiments of cell monolayer migration have revealed the spontaneous formation of finger-like instabilities, with leader cells at their tips. The mechanism driving this instability is still unknown at present. We present a particle-based model for collective cell migration, which includes velocity alignment interactions between neighboring cells. At the edge of the monolayer we introduce the following additional forces: surface-elasticity restoring force, curvature-dependent motility positive feedback, and contractile acto-myosin cables. We find that the curvature-driven instability at the layer edge is necessary and sufficient for the initiation of leader-cells and the subsequent growth of cellular fingers, which are in good agreement with experimental observations.

I. Introduction

Collective migration of cells occurs during the normal embryonic development process[1] and the physiological responses during wound healing or immune response.[2] It also plays an important role during pathologies such as cancer metastasis.[3] Therefore the mechanisms underlying collective cell migration are under intense current research.[4,5] Studies of collective cellular migration of a mono-layer on a flat surface have identified a form of edge instability, where the border of a cell layer develops finger-like extensions.[6–9] At the tips of such fingers highly motile "leader-cells" are observed, with a distinct morphology. The origin of this instability is still not understood, with several theoretical models proposed to explain the spontaneous formation of such cellular fingers.[10–15]

We investigate here the curvature-motility positive feedback mechanism, which was proposed in ref. 11. This mechanism is similar to the curvature driven instability implemented in the geometric model of crystal growth[16,17] in order to mimic in a simple way the Mullins–Sekerka instability.[18] We use a particle-based simulation, where cells are treated as point-particles, which was previously shown to describe very well the bulk dynamics of confluent cells.[19,20] This bulk model is then combined with a special treatment of the cells at the border (edge) of the cell layer: for convex regions (protrusions) we have an increasing motile force pulling the cell outwards, linearly increasing with the curvature.[11] This describes the phenomenological observation that cell motility is affected by the border curvature,[21] and the tendency of cells to extend larger and more frequent lamellipodia as their edge becomes more sharply curved.[22] For concave regions we add the contractile force due to the super-cellular acto-myosin cable that is observed to form at the layer edge,[9,23] and plays an important role during layer hole closure.[24–27] This model therefore allows us to explore the role of each of these components in the formation and dynamics of cellular fingers.

[a] Department of Chemical Physics, Weizmann Institute of Science, Rehovot 76100, Israel
[b] Mechanobiology Institute, National University of Singapore, Singapore
[c] Laboratoire de Physique Statistique, CNRS, Université P et M Curie, Université Paris Diderot, Ecole Normale Supérieure, Paris, France

† Electronic supplementary information (ESI) available. See DOI: 10.1039/c5ib00092k

II. The model

Our simulations are based on the model proposed in ref. 19, which is a particle-based model that includes Vicsek-type orientational interactions with pairwise effective potentials,[28] with the major change being the addition of specific forces that act on the cells that are in the outer edge of the cell layer. As described in ref. 19 the interactions between cells in our model exist only for nearest-neighbors. See the ESI† for a detailed description of the algorithm used to determine the nearest-neighbors and the border cells (see the ESI,† Fig. S1–S6). We specify below the different forces that act on the cells and determine their motion, within our model. Note that there are many other possible effects that contribute to cellular dynamics, which we have not investigated, such as the ability of cells to modify the properties of the substrate thereby allowing cells to have higher motility on such modified regions.[19]

A. Interaction potential

The basic inter-cellular interaction aims to mimic the following behavior of cells: when they are too close they repel, while they attract each other only when they are pulled apart beyond a certain separation. For cell–cell separations that are in between these two limits, the cells are considered to be rather compliant, certainly over the long time-scales of cellular motility, such that they do not effectively apply any forces on each other.

The resulting inter-cellular force is therefore taken to have magnitude[19]

$$F_{\text{interaction}}(r) = U_0 r \exp(-(r/A_0)^2) + U_2 \exp(-r/A_2) - U_3(r - A_3)^2 H(r - A_3) + U_1(r - A_1)H(r - A_1) \quad (1)$$

where $H(r)$ is the Heaviside function, r is the distance between two near-neighboring cells, and U_i,A_i are free parameters given in Table 1. The first two terms describe the short-range repulsion, while the last two terms describe the long-range attraction. Note that there is an upper limit on the separation between nearest-neighbor cells, taken to be 70 μm, beyond which they do not interact.

B. Random noise

Cells are self-propelled, performing a random walk when no other forces are applied on them. Hence we take a random force as an Ornstein–Uhlenback process with correlation time τ. The magnitude of the noise can depend on the local density of the cells, expressed by the following form[19]

$$\sigma(\rho) = \sigma_0 + (\sigma_1 - \sigma_0)\left(1 - \frac{\rho}{\rho_0}\right) \quad (2)$$

where ρ_0 is the reference density of the cells and ρ is the local cell density. The random force is directed along a direction $\vec{\eta}$, which evolves in time according to random diffusion in direction space, described by (for cell number i)

$$\tau \frac{\mathrm{d}\vec{\eta}_i}{\mathrm{d}t} = -\vec{\eta}_i + \vec{\xi}_i \quad (3)$$

where τ is the correlation time, and $\vec{\xi}_i$ is a delta-correlated white noise (independent for each cell): $\langle \xi_{j,\beta}(t)\xi_{i,\alpha}(t')\rangle = \delta_{i,j}\delta_{\alpha,\beta}\delta(t - t')$, where the index i describes the cell number and α the spatial direction.

Table 1 Table of all the parameters used in simulation

Variable	Value	Eqn	Variable	Value	Eqn
Max_NN_Dist	70 μm	Sup., ESI	τ	1.39 h	(3)
Θ_{hiding}	118°	Sup., ESI	α	1.42 h^{-1}	(4)
U_0	2650 h^{-2}	(1)	β	60 h^{-1}	(4)
A_0	8 μm	(1)	σ_0	150 μm $\text{h}^{-3/2}$	(2)
U_1	30 h^{-2}	(1)	σ_1	300 μm $\text{h}^{-3/2}$	(2)
A_1	2 μm	(1)	κ	2.5 μm^4 h^{-2}	(6)
U_2	2 μm h^{-2}	(1)	$F_{\max}$	1250 μm h^{-4}	(7)
A_2	25 μm	(1)	$H_{\max}$	0.05 μm^{-1}	(7)
U_3	1 h^{-2} μm^{-1}	(1)	F_{Cable}	350 μm h^{-2}	—
A_3	26 μm	(1)	T_0	35 h	(8)
DT	0.001 h	(S1), ESI	ρ_1	2.2 × 10^{-3} μm^{-2}	(8)

Sup. = appears in the ESI.

C. Vicsek interaction

Cells, like many other biological entities, tend to align their velocity when moving as a collective group. Mathematically this behavior is described here by a Vicsek-like/fluid viscosity term.[19,29] With this term we can write the overall equation of motion for a cell in our system as

$$\dot{\vec{v}}_i = -\alpha\vec{v}_i + \sigma(\rho)\vec{\eta}_i + \sum_{j\,\text{N.N.of}\,i}\left[\frac{\beta}{N_i}(\vec{v}_j - \vec{v}_i)\right] + \sum_{j\,\text{N.N.of}\,i}\left[\vec{F}_{\text{interaction},ij}(r_{ij})\right] \quad (4)$$

where α is the effective friction coefficient of the cell with the substrate, and β describes the strength of the orientational interactions with the nearest-neighboring cells. We work in the limit of zero inertia, so keeping forces in units of acceleration (mass is set to unity). In this limit the effective friction parameter α is describing the rate at which cells depolarize and reorient their internal polarization.

D. Contour forces

For the cells at the outer edge of the cell layer, we include several additional forces. First, there are passive restoring forces, which arise from the behavior of the edge as an effective one-dimensional membrane,[11] with a finite bending modulus κ (including the effect of cell thickness and typical lateral extent). There are two active forces at the edge: for a convex curvature there is a higher tendency of edge cells to form large lamellipodia pointing outwards, thereby producing a directed pulling force.[11] For a concave curvature, it is observed that cells tend to form an actin-myosin cable that acts to apply a large tension on the border cells. Such a cable is observed during hole closure experiments, as a "purse-string" mechanism.[24–27]

The restoring force of the effective 1D membrane is described by a Helfrich energy functional

$$\mathcal{F} = \int\left(\frac{1}{2}\kappa H^2\right)\mathrm{d}s \quad (5)$$

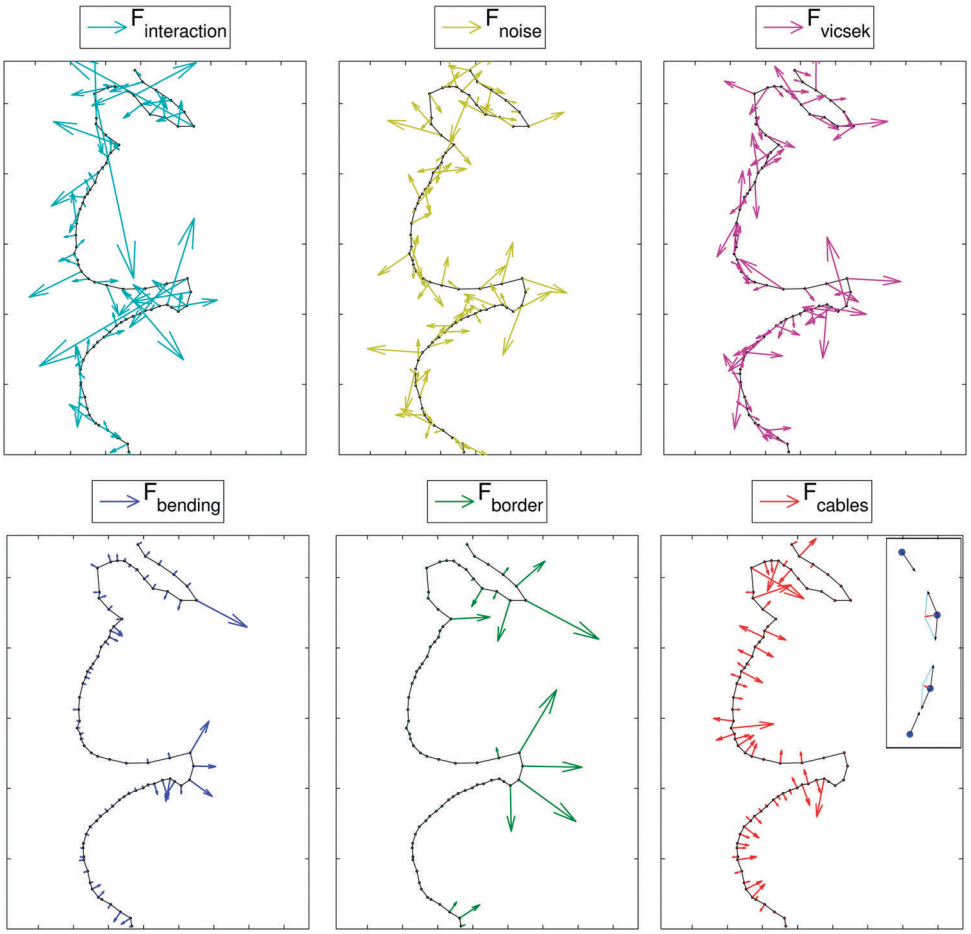

Fig. 1 A snapshot of an evolving border of the expanding cell layer, indicating the magnitude and directions of the local normal forces at the edge (all forces are plotted with the same scale): $\vec{F}_{\text{interaction}}$ (eqn (1), fourth term in eqn (4)), $\vec{F}_{\text{noise}}$ (second term in eqn (4)), $\vec{F}_{\text{vicsek}}$ (third term in eqn (4)), the restoring force due to curvature $\vec{F}_{\text{bending}}$ (eqn (6)), the active lamellipodia-driven force acting on the convex regions $\vec{F}_{\text{border}}$ (eqn (7), always pointing towards the outwards normal), and finally the force arising from the contractile acto-myosin cable acting in the concave regions $\vec{F}_{\text{cable}}$. The inset shows how the local tangential forces $\vec{F}_{\text{cable}}$ between the cells that make up the cable, end up pulling the cells in the normal direction, due to the local curvature.

where H is the magnitude of the local curvature of the border contour (see the ESI,† Fig. S8 and S9). The normal forces applied on the border cells are derived from the Helfrich energy, to be[11]

$$\vec{F}_{\text{bending}} = -\kappa\frac{\mathrm{d}^2\vec{H}}{\mathrm{d}s^2} + \frac{3}{2}\kappa|H|^2\vec{H} \qquad (6)$$

shown in Fig. 1.

Cells at the layer edge tend to extend larger lamellipodia towards the open surface, inducing a large pulling force directed outwards.[30] The active force describing the positive feedback between convex curvature ($H < 0$) at the border and increased motile force of the cells is given by[11]

$$F_{\text{border}}\begin{cases} F_0 & H > 0 \\ \dfrac{F_{\max}}{H_{\max}}|H| & 0 > H > -H_{\max} \\ F_{\max} & H < -H_{\max} \end{cases} \qquad (7)$$

where $H_{\max} \simeq (20)^{-1}$ $(\mu\text{m})^{-1}$ is the maximal curvature that the cells can adopt, with the corresponding maximal motile force $F_{\max}$, and $F_0 = 0$ is the outwards directed motile force on border cells in flat or concave regions. This force always points towards the outwards normal to the border contour (Fig. 1).

Note that in Fig. 1 the patterns of $\vec{F}_{\text{bending}}$ and $\vec{F}_{\text{border}}$ are somewhat similar in the fingers. However, the origin of this behavior is very different: the bending force is attempting to inflate the sharp tip of the finger so as to reduce its local curvature, due to the H^3 term in eqn (6) (last term). The bending force of eqn (6) can never be the source of fingers and instability, as it acts initially to flatten any initiation of undulations in the edge contour. By contrast, the active force of cell motility described by $\vec{F}_{\text{border}}$ is linear in curvature H (eqn (7)), and is indeed the sole driver of the fingers' instability in our model.

The actin cables are modeled as an additional attraction force ($\vec{F}_{\text{cable}}$) that acts between border cells, pulling them towards each other, as long as the local border contour curvature is concave ($H > 0$, Fig. 1). The value of $F_{\text{cable}} = 350$ $(\mu\text{m h}^{-2})$ was chosen to give a good fit to the observed dynamics (Fig. 4a), and also agrees with estimates based on hole-closure experiments.[5] These acto-myosin cables are observed to inhibit the formation of

outwards-pointing lamellipodia in the edge cells,[9] which in our model appears naturally through the distinct division between $\vec{F}_{\text{border}}$ and $\vec{F}_{\text{cable}}$ based on the sign of the curvature (eqn (7)).

E. Proliferation

Cells in the model divide at an average constant rate, with a mean division time of $\langle T \rangle \sim 28$ h. We implement the observation that cell division time depends on the local cell density,[31] by the following expression

$$T(\rho) = T_0\left(1 + \left(\frac{\rho}{\rho_1}\right)^4\right) \quad (8)$$

where ρ_1 is some reference density, and T_0 is a model parameter chosen to fit the real division time (Table 1).

III. Results

A. Finger formation

We begin by fitting the key parameters of the model, so that we have good agreement (Fig. 2a) with the observations of finger instability in expanding cell layers.[6–9] Note that while the model is general, we wish to explore a realistic range of parameters, and therefore it was useful to first fit it to the observed behavior of one particular cell type (MDCK cells). We used essentially the same parameter set that was found in ref. 19, which fits the

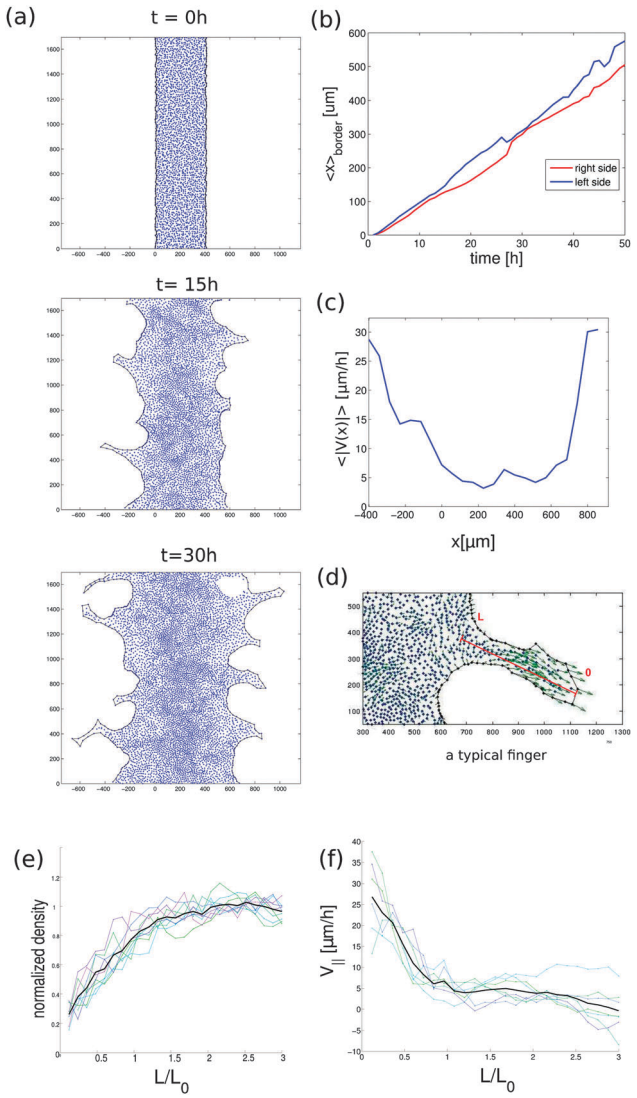

Fig. 2 (a) Typical shapes of an expanding cell layer at the indicated times, exhibiting the fingers' instability (using the nominal values of the parameters given in Table 1). (b) Mean value of the $|x|$-coordinate displacement of the border cells, as a function of time. The expansion is roughly linear. (c) Mean cell speed across the layer, as a function of the x-coordinate, at time $t = 22$ h (see (a)). (d) Typical shape of a growing finger, showing the velocity field of the cells. Also indicated is the main axis of the finger (red line), which is used to extract (e) the mean cell density and (f) the mean cell parallel velocity (along the finger axis), averaged over the finger cross-section.

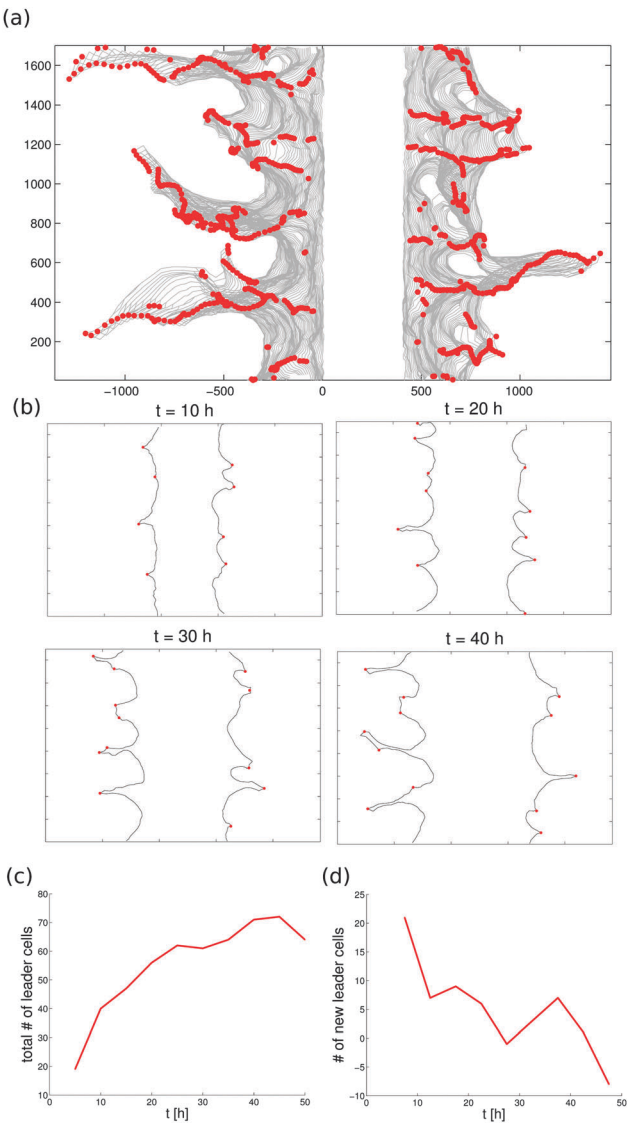

Fig. 3 (a) Overlay of the border contour of the expanding cellular layer (grey lines) with the leader-cells marked in red. (b) Snapshots of the simulation shown in (a), for the indicated times. (c) Total number of leader-cells along an accumulated 17 mm length of initial contour edge, as a function of time. (d) The rate of initiation of new leader-cells (every 5 h), for the same simulations as in (c).

bulk behavior of the cell layer. The remaining parameters relate to our application of the shape-motility model on the outer contour, and these are fitted to the observations as follows. The overall density of fingers along the contour is described by the linear stability analysis which gives the wavelength of the most unstable mode[11] (λ_{finger}, eqn (S10), ESI†). We find that in our model this relation still describes very well the average distance between fingers (Fig. S10, ESI†). Note that the appearance of the fingers is a stochastic event due to the random motion of the cells, with λ_{finger} giving the average separation. To fit the calculated density of fingers to the observations, we fix κ, such that: $\lambda_{finger} \sim 300$ μm. However, this length-scale depends on the ratio of the effective bending modulus of the contour, and the slope of the curvature-force feedback (F_{max}). We vary F_{max}, while keeping the density of fingers fixed, until we find fingers that have maximal velocities for their leader-cells (at the tips, Fig. 2f) that match the observed values of $V_{tip} \sim 20$ μm h^{-1}.[19] We also avoided very large values of F_{max} where cells at the tips of fingers begin to detach from the confluent layer (Fig. S7, ESI†), if F_{max} is larger than the attractive force from the inter-particle potential (eqn (1)). The final set of parameters is given in Table 1.

Using these parameters we find indeed that our model gives rise to the spontaneous initiation and elongation of fingers (Fig. 2a). The overall density of fingers along the edge of the cell layer, as well as the time-scale of the motion of the contour (Fig. 2b), is in good agreement with the observations.[19] In Fig. 2c we plot the calculated mean velocity profile, which is in good agreement with observations.[7] Note that in the experiments the contour velocity is observed to increase linearly with time, until it reaches a finite terminal value,[6,19] while we calculate a finite contour velocity from the beginning. This may arise due to some incubation time for the cells to respond to the appearance of the free edge and for them to form lamellipodia that extend into this open space.

A more detailed analysis of the finger itself is shown in Fig. 2d–f. We find that the cells have a highly ordered flow within the finger (Fig. 2d), as was observed,[7,8] corresponding to the velocity profile shown in Fig. 2e, for several typical fingers. The cell density is found to decrease along the finger (Fig. 2e), again in very good agreement with experimental observations.[8]

An additional comparison to experiments is for the overall rate of formation of leader-cells along the edge of the expanding cellular layer. This was measured in experiments (Fig. S9, ESI† [19]), and we find in our simulations a very similar trend (Fig. 3). Both the overall density of the leader-cells as well as their rate of formation match very well the observations. We identify here leader-cells as particles at the free edge that have a convex curvature that is larger than some minimal threshold (see details in the ESI†). Note that the rate of initiation of new leader-cells can become negative at long times (Fig. 3d) due to coalescence of fingers.

We therefore conclude that the model we propose gives a realistic account of the dynamics of the cells in the expanding layer, including the finger instability at the outer edge.

We next explored systematically the components of the model for their effect on the formation of fingers. As shown in Fig. S11b (ESI†), cell proliferation is not essential for the initiation of fingers. However, the lack of new cells eventually limits very strongly the ability of the layer to expand, and of the fingers to

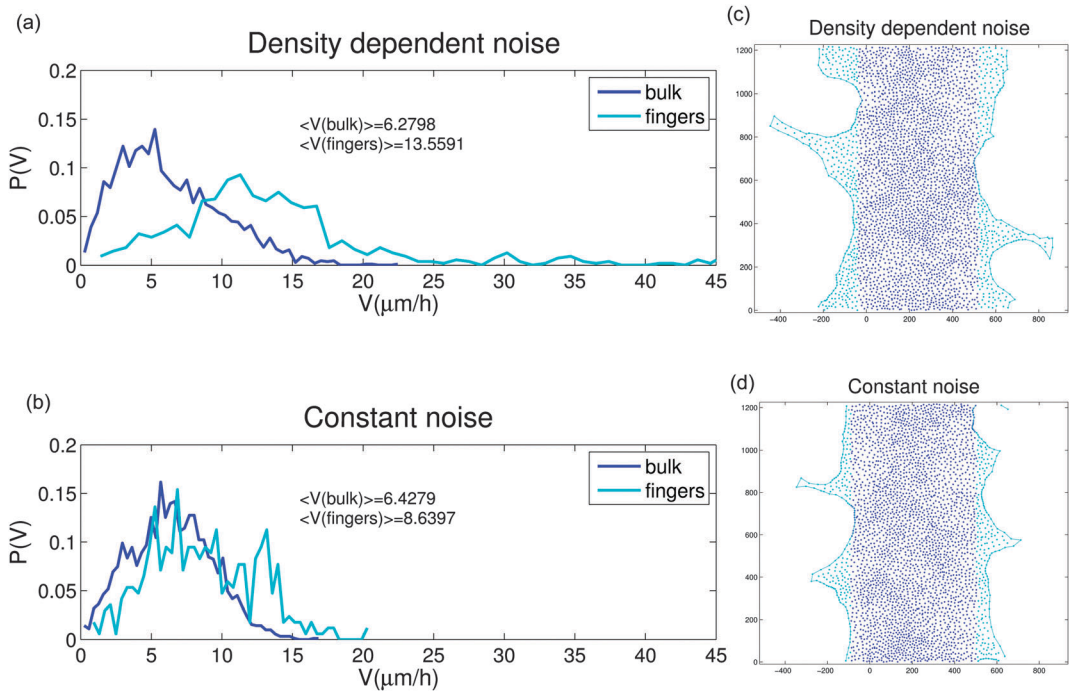

Fig. 4 (a and b) Velocity distributions in the bulk (dark blue) and fingers (light blue) for the density dependent and independent noise cases. (c and d) Snapshot at t = 20 h for finger formation with density dependent and independent noise (eqn (2)). The bulk cells are indicated in dark blue, while those related to the fingers are indicated in light blue.

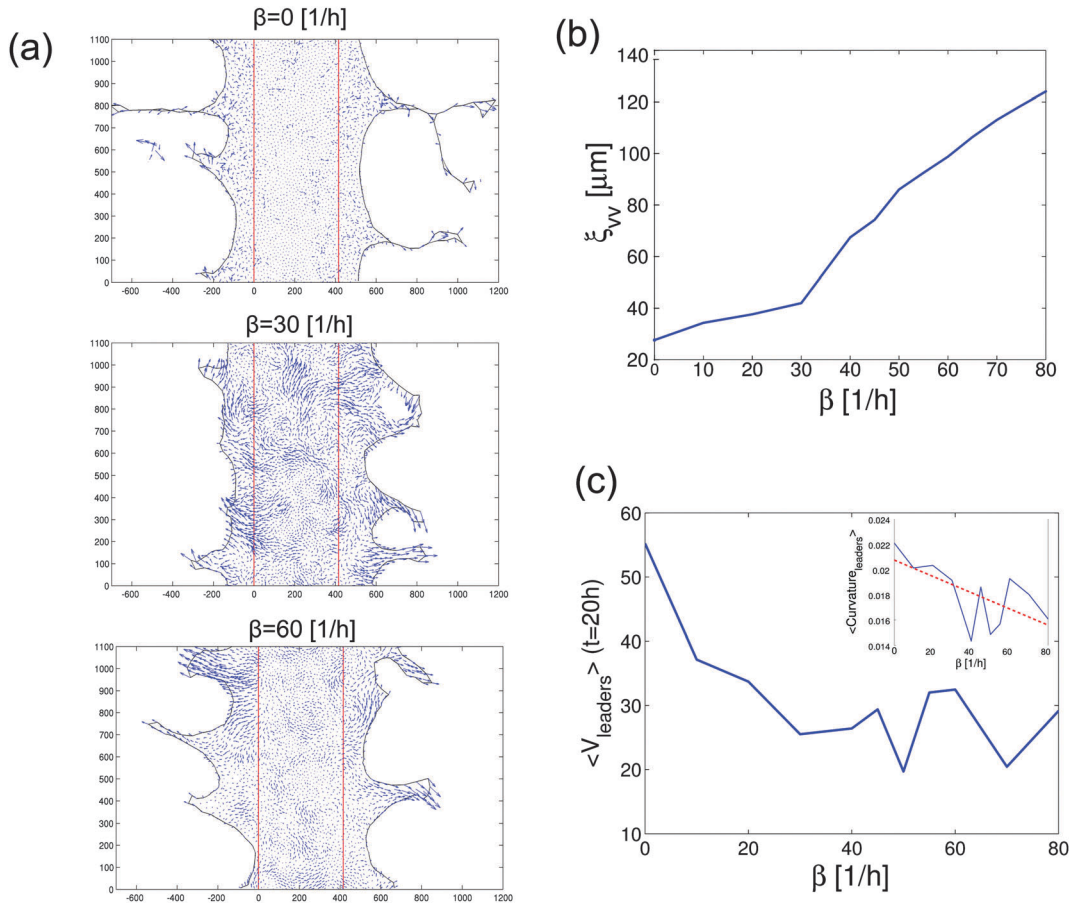

Fig. 5 (a) Typical shapes and velocity fields of expanding cell layers (t = 20 h), calculated for different values of the orientational (Vicsek-like) interaction β (eqn (4)). (b) Velocity correlation lengths ξ_{vv} in the layer bulk as a function of β from the simulations, showing the monotonic increase with β. (c) The mean velocity of the leader-cells (see Fig. 3 for leader-cell detection), and their curvature, as a function of β.

continue growing. In Fig. 4 we explore the role of density-dependent noise ($\sigma_1 - \sigma_0$ in eqn (2)[19]) in the formation of fingers. We find that while fingers initiate even with a uniform noise ($\sigma_0 = \sigma_1$), they tend to be thicker and smaller in amplitude (Fig. 4a). More importantly, the lower noise at the edge of the density-independent noise prevents the cells following the leader from being able to move fast and keep up, thereby acting to slow down the finger growth significantly. In Fig. 4b we compare the velocities of the cells inside the fingers, and find that without the density-dependent noise they are similar to the bulk, while with density dependent noise they are much faster, as observed in experiments. We therefore conclude that this element is important to allow the cells behind the leader to be able to follow its fast velocity.[19]

B. Role of orientational ordering

We wanted to explore the role played by the tendency of cells to align their motion with that of their neighboring cells, in the formation of fingers (Fig. 5a). First, when varying the alignment parameter β (eqn (4)) in our model we also affect the overall motility inside the bulk cell layer, such that it is reduced when β is increased (Fig. S12, ESI†). We therefore adjusted the noise level (σ) to recover the observed velocity distribution in the bulk (Fig. S12, ESI†). As shown in Fig. 5a, the alignment parameter strongly affects the shape of the fingers, such that they become very narrow for small values of β. The reason for this is the reduction in the velocity correlation length ξ_{vv} (Fig. S13b, ESI†) with decreasing β (Fig. 5b), such that a leader-cell cannot induce a large flow of followers when the correlation length is too small. The result is that cells follow the leader in a single-file manner, and the finger becomes very thin. Since the fingers are thinner for smaller β they tend to have a higher curvature at their tips, and faster leader-cells (Fig. 5c).

For large values of β we find that the leaders induce large flows of followers (Fig. 5a), which results in thicker fingers. In the limit of large values of β the correlation length ξ_{vv} grows to the size of the whole layer,[32] and in principle the cells would begin to behave as a highly correlated "flock", in which they are perfectly aligned with the leaders. In this limit we expect very few (but very wide) fingers, since the whole layer simply moves coherently in the same direction.

In a simple contour model for this instability,[11] fingers grew whenever the contour became unstable, since in that model the motion of the contour was not impeded by the cellular flow in the bulk, which was not described. We find here that for the contour-driven instability to form, the cells in the bulk need to

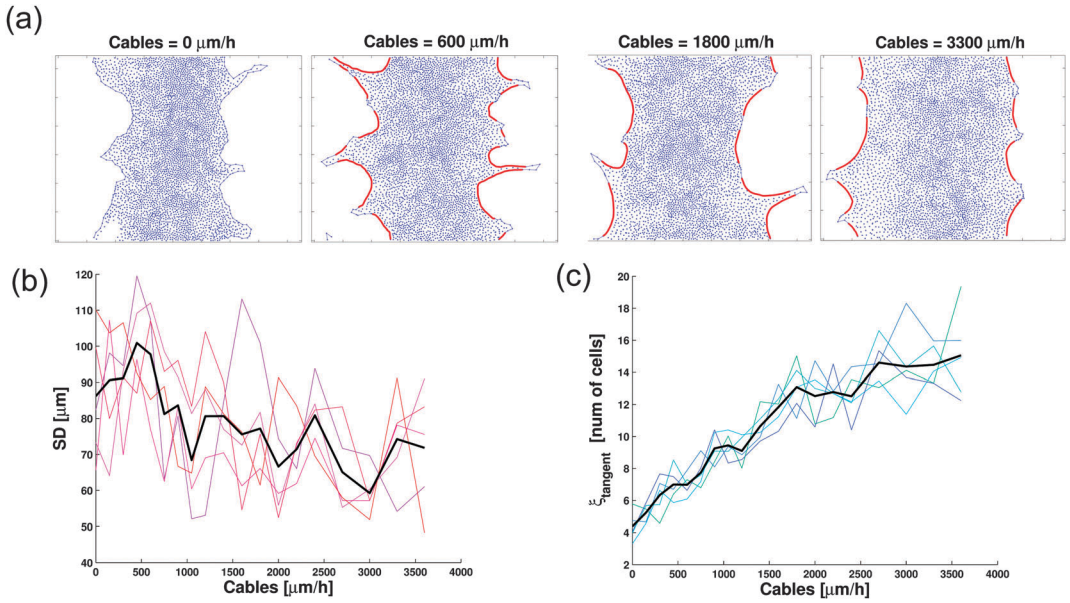

Fig. 6 (a) Typical shapes of expanding cell layers, calculated for different values of the acto-myosin cable tension F_{cable}. The parts of the contour which are concave and contract due to the cable are denoted by red lines. (b) Average roughness (SD) of the border contour, as a function of the cable force. We find that increasing cable tension tends to flatten the contour. In (c) this is observed as an increase in the tangent correlation length along the contour.

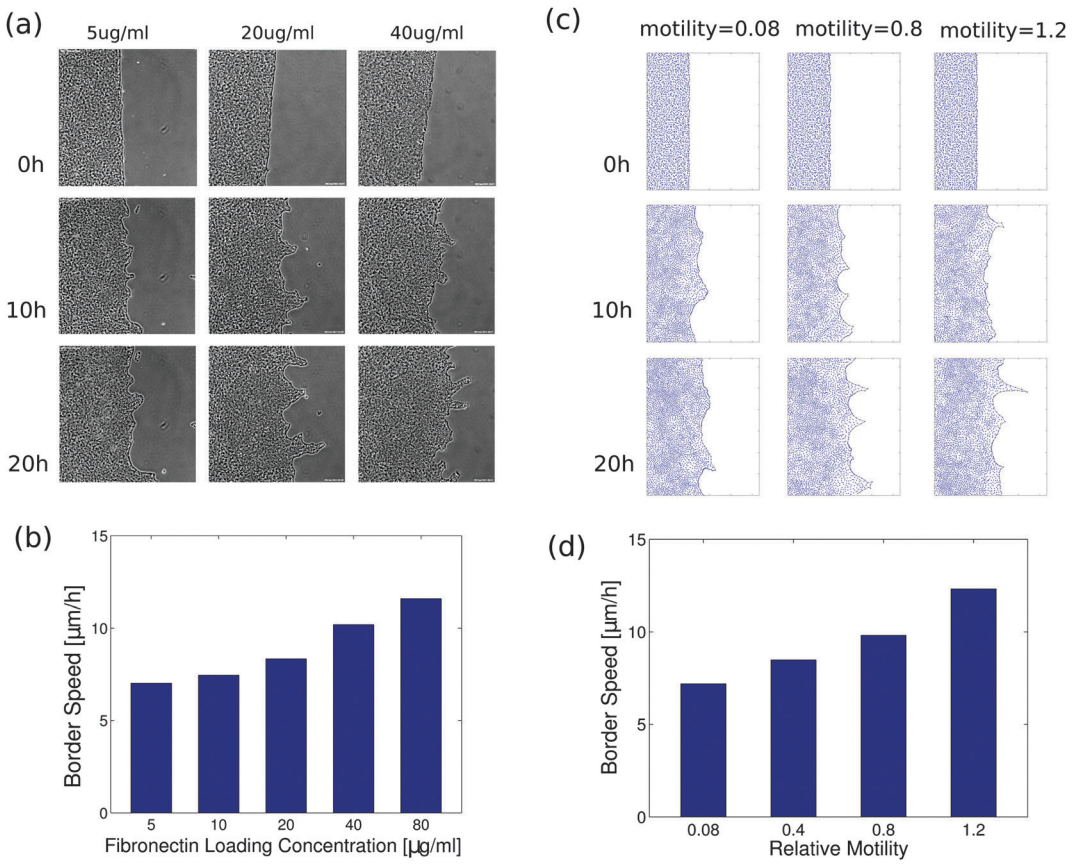

Fig. 7 (a) Typical shapes of expanding cell layers, in experiments using the indicated concentration of fibronectin coating. The expansion is faster for larger fibronectin concentration, as shown by the mean border velocity (b). (c) Simulations using different values of the ''motility factor'' which changes the motility of the leader-cells (F_{max}, eqn (7)) by a scaling factor. The qualitative similarity is very good, showing that fingers form only above a threshold of leader-cell motility, as is also seen in the mean border velocity (d).

be recruited into the growing fingers, and this can happen only when they have strong enough alignment interactions. Otherwise, the flow of cells behind the leaders is limited to the base of the finger, in a single-file manner, resulting in very thin fingers.

C. Acto-myosin cables at the border contour

Another distinct feature appearing at the edge of cell layers is a supracellular actomyosin cable that contracts the cells.[9,23] This feature plays an important role during the closure of holes in the cell layer,[24–26] in a purse-string mechanism. In the experiments it is observed that this cable appears only in regions where the edge has a concave shape. We have implemented this additional contractility of the edge cells, when they have a concave shape, and explored the role of this feature in the formation and shapes of the fingers. In Fig. 6a we plot the shape of typical cell layers for different values of cable tension F_{cable}. We find that the tension in the cable adds to the line-tension at the layer edge that acts to suppress the fingers,[11] leading to a lower density of fingers along the contour (increasing $\lambda_{\mathrm{finger}}$, eqn (S10), ESI†). In addition, by pulling the cells in the concave regions outwards, the cable tension leads to faster overall layer expansion.

These qualitative features are manifested in the diminishing amplitude of fingers with increasing cable tension, as shown in Fig. 6b. Similarly, the effect of the cable to lower the density of fingers and smoothen the outer contour results in an increasing correlation length along the contour ξ_{tangent} (Fig. 6c and Fig. S13a, ESI†). Our model therefore predicts that inhibiting the formation of the actomyosin cable at the layer edge will induce a proliferation of fingers, but slower overall border expansion.

Note that the role of myosin contractility in the edge motion is not only through its effect on the tension in the acto-myosin cables, which we study in Fig. 6. As was observed in experiments,[30,33,34] reducing contractility using blebbistatin results in enhanced overall cellular motility, with larger and more persistent lamellipodia. This effect can of course enhance the advance of the edge, and dominate over the effects of the cables that we describe in Fig. 6.

IV. Effects of motility and comparison with experiments

To study the effects of overall cell motility on the finger formation, experiments were carried out with different concentrations of fibronectin coating (Fig. 7a, see the ESI† for details). It is found that overall cell layer expansion increases with the fibronectin concentration, due to stronger cell–substrate adhesion and larger traction forces, as shown by the mean border progression (Fig. 7b). We show in Fig. 7c and d that a very similar behavior is found using our model, where we increase the motility of the leader-cell force (F_{max}, eqn (7)). When we vary the simulations of

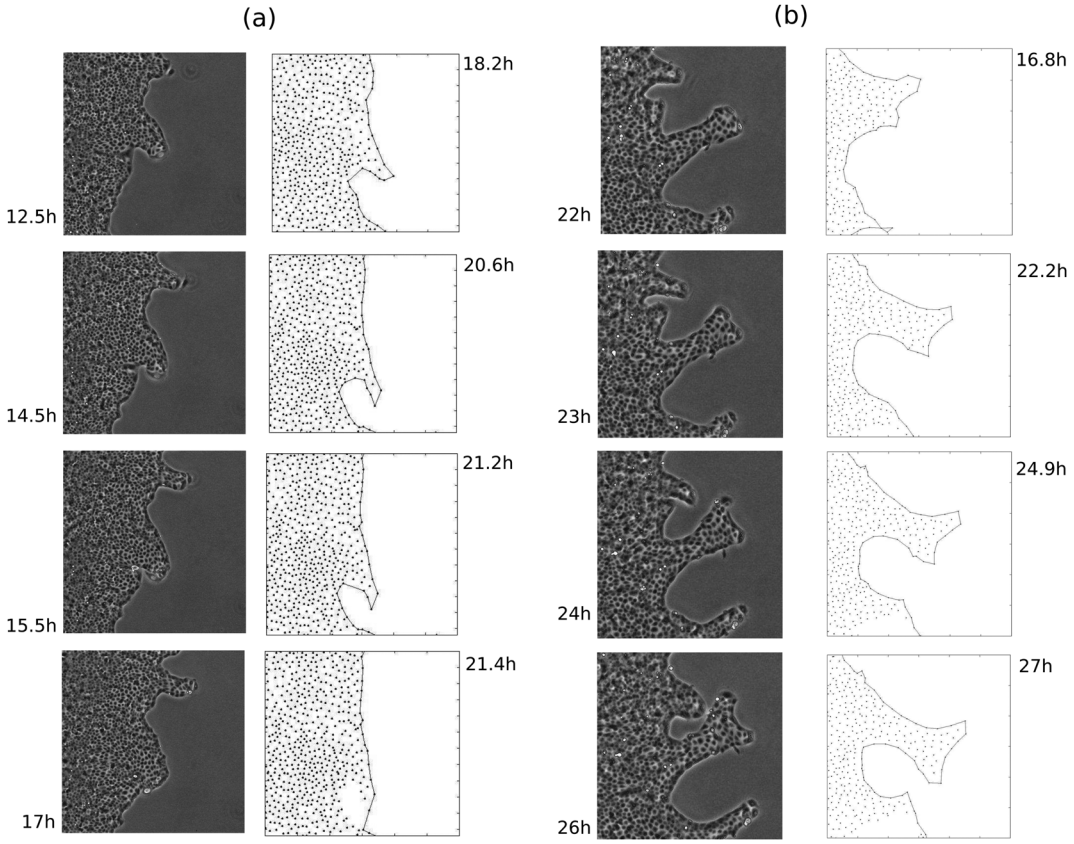

Fig. 8 (a) Example from experiments (left column) and simulations (right column) of the evolution of a finger of cells that moves side-ways and eventually bends and curves backwards until it merges with the main cell layer. (b) An example of a finger undergoing a tip-splitting event, in experiments (left) and simulations (right).

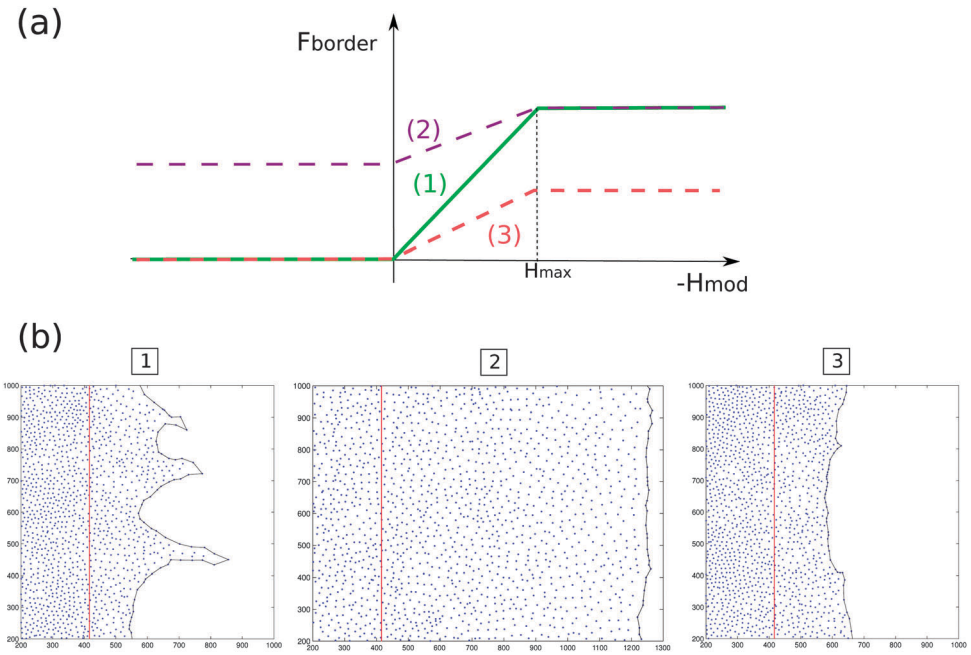

Fig. 9 A schematic illustration of the relation between F_{border} and the curvature of the edge, that we use in this work (denoted by the green line (1), eqn (7)). For a large enough positive slope we predict fingers, while for the two cases indicated by dashed lines (2 and 3) we do not find fingers, as shown in the simulations below.

both the leader-cell force and the overall noise magnitude (σ_0, σ_1, eqn (2)), we find that the increase in border progression is larger than that observed. The fibronectin coating therefore seems to affect most strongly the motility of the leader-cells, rather than the random motility within the bulk of the layer.

Note that the observed increase in motility (cell velocity) with the concentration of the fibronectin coating (Fig. 7) is eventually reversed in experiments on single cell motility.[35,36] The reason is that with the increase in cell–substrate adhesion not only the traction forces increase, but also the effective friction coefficient α in eqn (4) (or the rate of cell loss of polarization). This leads us to expect the cells to slow down for very high fibronectin concentrations, where they essentially become adherent and non-motile.

In Fig. 8 we compare different qualitative behaviors of the fingers, observed both in the experiments and in our simulations. We often observe in the simulations that the fingers can bend and curve backwards towards the bulk layer (Fig. 8a), and this is also observed in experiments. One mechanism driving this dynamics is the contraction of the acto-myosin cable, which acts more strongly on the more highly curved side of the finger. Fig. 8b shows a finger undergoing a tip-splitting event. Unlike the continuum model,[11] where the tip-splitting was unavoidable and happened for all fingers, in the discrete model we find that these events are greatly suppressed, as observed in experiments.

V. Conclusion

In this work we demonstrated that the instability of an expanding cell monolayer for the formation of cellular fingers can be described by a theoretical model that contains two essential ingredients: leader-cells are initiated through the positive feedback between the protrusion of a cell at the layer edge and its motility, and such leaders are then able to direct a cohort of followers behind them due to orientational interactions.

In Fig. 9 we summarize the different cases that are often encountered in expanding cellular layers. For the case indicated by (1) we have a strong positive feedback between the curvature and the motile force, which initiates fingers.[11] For such fingers to be able to thicken and grow the cells need to have strong enough orientational interactions. (2) For highly motile cells, such that irrespective of the curvature at the edge they extend lamellipodia and crawl outwards, we have a weak curvature-motility feedback, and do not expect fingers to form. This is indeed observed for fast migrating cell layers.[37] When the positive feedback is too weak due to overall low cell motility (case 3), we again do not predict finger formation, as is indeed observed experimentally (Fig. 7). Another feature that has been observed in several experiments, mostly when fingers do not form (as in case 2), is of waves of acceleration that propagate from the monolayer edge into the bulk.[34,37,38] We find somewhat similar waves in our system (Fig. S14, ESI†), although a detailed study of this phenomenon is beyond the scope of this paper.

Our work allows for a systematic exploration of this collective instability phenomenon, and makes quantitative predictions that are verified by experiments. The model can be used in other configurations, and for different geometries. By extracting the cellular properties essential for the fingering phenomenon, our work gives motivation for studies aimed at uncovering the underlying molecular processes behind collective migration,[39,40] which are still not fully known at present.

Acknowledgements

We thank Pascal Silberzan for motivating this study and guidance along the way. NSG would like to acknowledge the Institute Curies Mayent-Rothschild Visiting Professor fund and Labex CelTisPhyBio for their support during the stay at the Institute Curie, where this research was initiated. N.S.G is the incumbent of the Lee and William Abramowitz Professorial Chair of Biophysics, and would like to thank also the ISF grant 580/12 for support. This work is made possible through the historic generosity of the Perlman family.

References

1 P. Rørth, *EMBO Rep.*, 2012, **13**, 984.
2 P. Friedl and D. Gilmour, *Nat. Rev. Mol. Cell Biol.*, 2009, **10**, 445.
3 P. Friedl, J. Locker, E. Sahai and J. E. Segall, *Nat. Cell Biol.*, 2012, **14**, 777.
4 S. R. K. Vedula, A. Ravasio, C. T. Lim and B. Ladoux, *Physiology*, 2013, **28**, 370.
5 N. S. Gov, in *Cell and Matrix Mechanics: Collective Cell Migration*, ed. R. Kaunas and A. Zemel, CRC Press, 1st edn, 2014.
6 M. Poujade, E. Grasland-Mongrain, A. Hertzog, J. Jouanneau, P. Chavrier, B. Ladoux, A. Buguin and P. Silberzan, *Proc. Natl. Acad. Sci. U. S. A.*, 2007, **104**, 15988.
7 L. Petitjean, M. Reffay, E. Grasland-Mongrain, M. Poujade, B. Ladoux, A. Buguin and P. Silberzan, *Biophys. J.*, 2010, **98**, 1790.
8 M. Reffay, L. Petitjean, S. Coscoy, E. Grasland-Mongrain, F. Amblard, A. Buguin and P. Silberzan, *Biophys. J.*, 2011, **100**, 2566.
9 M. Reffay, M.-C. Parrini, O. Cochet-Escartin, B. Ladoux, A. Buguin, S. Coscoy, F. Amblard, J. Camonis and P. Silberzan, *Nat. Cell Biol.*, 2014, **16**, 217.
10 G. Y. Ouaknin and P. Z. Bar-Yoseph, *Biophys. J.*, 2009, **97**, 1811.
11 S. Mark, R. Shlomovitz, N. S. Gov, M. Poujade, E. Grasland-Mongrain and P. Silberzan, *Biophys. J.*, 2010, **98**, 361.
12 E. Khain, M. Katakowski, N. Charteris, F. Jiang and M. Chopp, *Phys. Rev. E: Stat., Nonlinear, Soft Matter Phys.*, 2012, **86**, 011904.
13 M. H. Köpf and L. M. Pismen, *Soft Matter*, 2013, **9**, 3727.
14 M. BenAmar, *Eur. Phys. J. E: Soft Matter Biol. Phys.*, 2013, **36**, 1.
15 M. Basan, J. Elgeti, E. Hannezo, W.-J. Rappel and H. Levine, *Proc. Natl. Acad. Sci. U. S. A.*, 2013, **110**, 2452.
16 R. C. Brower, D. A. Kessler, J. Koplik and H. Levine, *Phys. Rev. A: At., Mol., Opt. Phys.*, 1984, **29**, 1335.
17 D. A. Kessler, J. Koplik and H. Levine, *Phys. Rev. A: At., Mol., Opt. Phys.*, 1984, **30**, 3161.
18 J. Langer, *Rev. Mod. Phys.*, 1980, **52**, 1.
19 N. Sepúlveda, L. Petitjean, O. Cochet, E. Grasland-Mongrain, P. Silberzan and V. Hakim, *PLoS Comput. Biol.*, 2013, **9**, e1002944.
20 M. Deforet, V. Hakim, H. Yevick, G. Duclos and P. Silberzan, *Nat. Commun.*, 2014, **5**, 3747.
21 C. G. Rolli, H. Nakayama, K. Yamaguchi, J. P. Spatz, R. Kemkemer and J. Nakanishi, *Biomaterials*, 2012, **33**, 2409.
22 S. Rausch, T. Das, J. R. Soiné, T. W. Hofmann, C. H. Boehm, U. S. Schwarz, H. Boehm and J. P. Spatz, *Biointerphases*, 2013, **8**, 32.
23 J. K. Klarlund, *Proc. Natl. Acad. Sci. U. S. A.*, 2012, **109**, 15799.
24 E. Anon, X. Serra-Picamal, P. Hersen, N. C. Gauthier, M. P. Sheetz, X. Trepat and B. Ladoux, *Proc. Natl. Acad. Sci. U. S. A.*, 2012, **109**, 10891.
25 A. Brugués, E. Anon, V. Conte, J. H. Veldhuis, M. Gupta, J. Colombelli, J. J. Muñoz, G. W. Brodland, B. Ladoux and X. Trepat, *Nat. Phys.*, 2014, **10**, 683.
26 O. Cochet-Escartin, J. Ranft, P. Silberzan and P. Marcq, *Biophys. J.*, 2014, **106**, 65.
27 S. R. K. Vedula, G. Peyret, I. Cheddadi, T. Chen, A. Brugués, H. Hirata, H. Lopez-Menendez, Y. Toyama, L. N. de Almeida and X. Trepat, *et al.*, *Nat. Commun.*, 2015, **6**, 6111.
28 H. Chaté, F. Ginelli, G. Grégoire, F. Peruani and F. Raynaud, *Eur. Phys. J. B*, 2008, **64**, 451.
29 T. Vicsek, A. Czirók, E. Ben-Jacob, I. Cohen and O. Shochet, *Phys. Rev. Lett.*, 1995, **75**, 1226.
30 R. Farooqui and G. Fenteany, *J. Cell Sci.*, 2005, **118**, 51.
31 A. Puliafito, L. Hufnagel, P. Neveu, S. Streichan, A. Sigal, D. K. Fygenson and B. I. Shraiman, *Proc. Natl. Acad. Sci. U. S. A.*, 2012, **109**, 739.
32 G. Grégoire and H. Chaté, *Phys. Rev. Lett.*, 2004, **92**, 025702.
33 Z. Liu, L. A. van Grunsven, E. Van Rossen, B. Schroyen, J.-P. Timmermans, A. Geerts and H. Reynaert, *Br. J. Pharmacol.*, 2010, **159**, 304.
34 Y. Matsubayashi, W. Razzell and P. Martin, *J. Cell Sci.*, 2011, **124**, 1017.
35 S. R. Peyton and A. J. Putnam, *J. Cell. Physiol.*, 2005, **204**, 198.
36 S. L. Gupton and C. M. Waterman-Storer, *Cell*, 2006, **125**, 1361.
37 A. Zaritsky, D. Kaplan, I. Hecht, S. Natan, L. Wolf, N. S. Gov, E. Ben-Jacob and I. Tsarfaty, *PLoS Comput. Biol.*, 2014, **10**, e1003747.
38 X. Serra-Picamal, V. Conte, R. Vincent, E. Anon, D. T. Tambe, E. Bazellieres, J. P. Butler, J. J. Fredberg and X. Trepat, *Nat. Phys.*, 2012, **8**, 628.
39 T. Das, K. Safferling, S. Rausch, N. Grabe, H. Boehm and J. P. Spatz, *Nat. Cell Biol.*, 2015, **17**, 276.
40 E. Bazelliéres, V. Conte, A. Elosegui-Artola, X. Serra-Picamal, M. Bintanel-Morcillo, P. Roca-Cusachs, J. J. Muñoz, M. Sales-Pardo, R. Guimerá and X. Trepat, *Nat. Cell Biol.*, 2015, **17**, 409.

